# Chapter 9

# Coronal mass ejections

## 9.1 Basic concepts and observational constraints

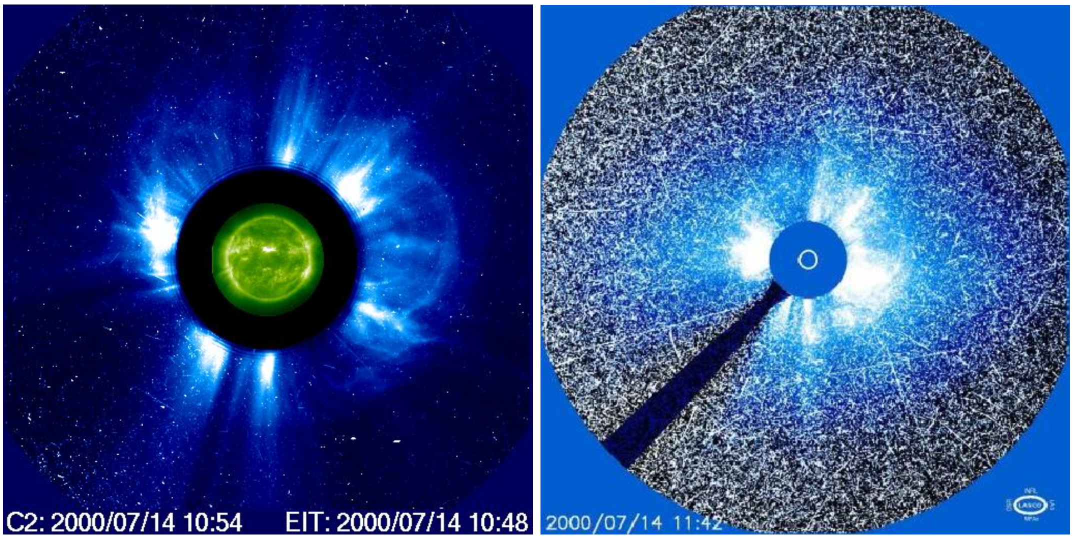


Figure 9.1: CMEs are observed with coronagraphs that block emission from the bright solar disk (SOHO LASCO images).

CME characteristics:

- Observed in white light (Thomson scattering of sunlight from electrons)
- Observed CME speeds $\sim$ 10 – 3000 km/s
- Typical CME mass $2{\times}10^{14}$ – $4{\times}10^{16}$ g
  (solar mass $2{\times}10^{33}$ g)
- Different sizes and shapes
- Activity maximum: several CMEs per day
  Activity minimum: one per week or less

For speed determination, we need to

- define the CME front
- consider that these are plane-of-the-sky observations
- remember that CME speed consists of expansion velocity + propagation velocity

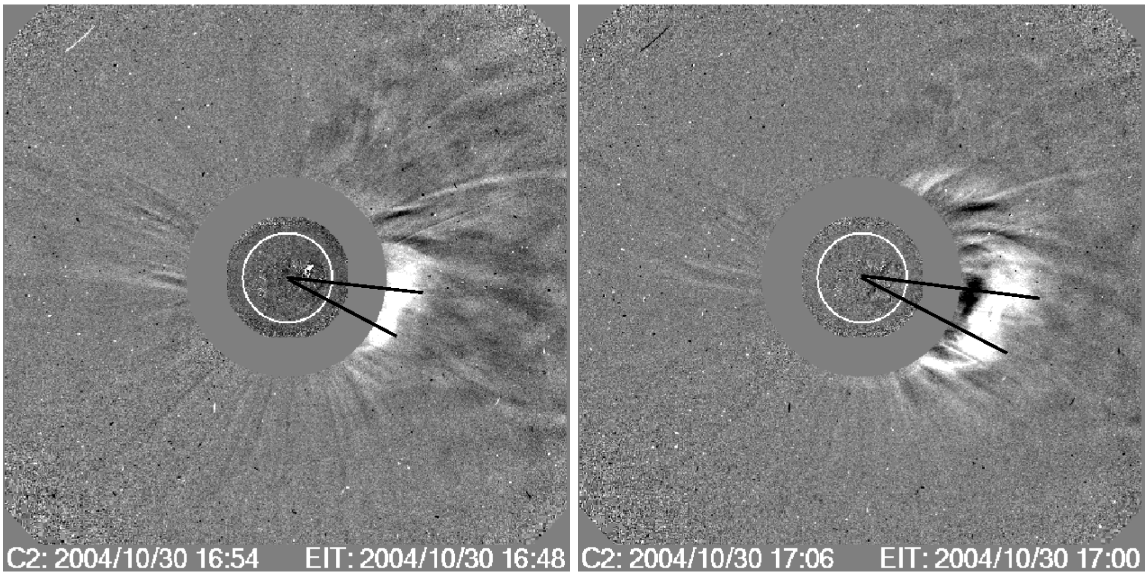


Figure 9.2: Consecutive CME difference images for CME front speed determination.

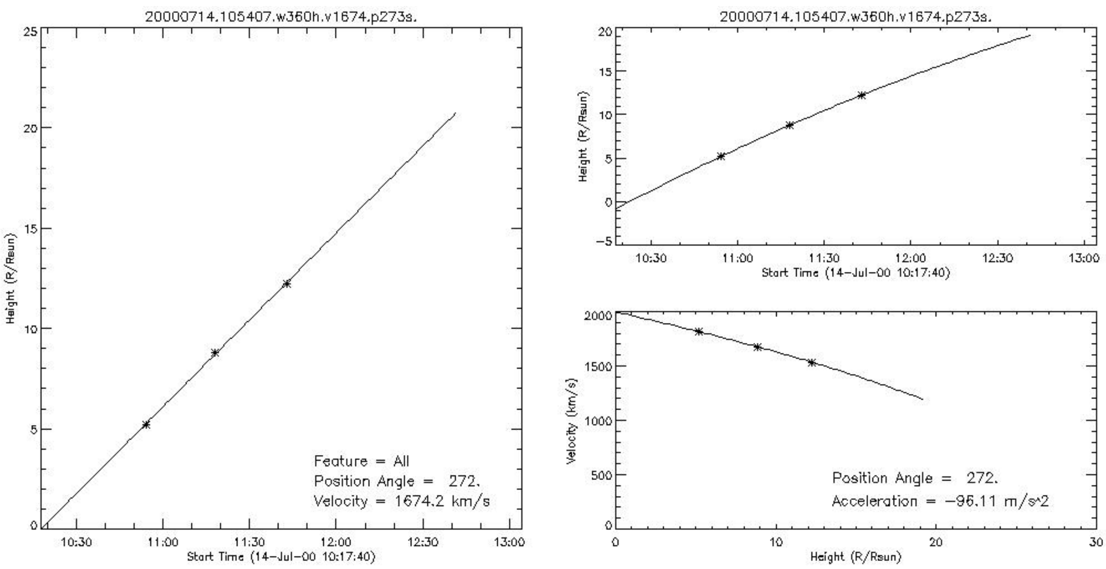


Figure 9.3: Height-time plot from the LASCO CME Catalog (on the left), and the estimated speed based on a second-order fit (on the right). The solar limb is at $R = 1\,R_\odot$.

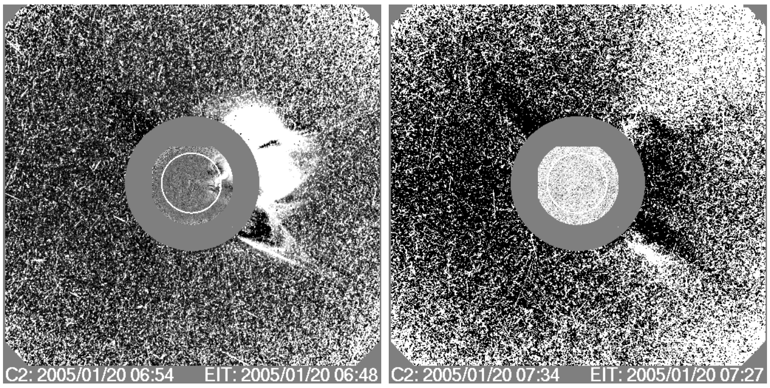


Figure 9.4: In many cases we simply lack good data: Halo CME first observed at 06:54 UT, flare X7.1 in AR N14W61, protons and lots of particle hits (left). However, the next available image (right) does not give much information.

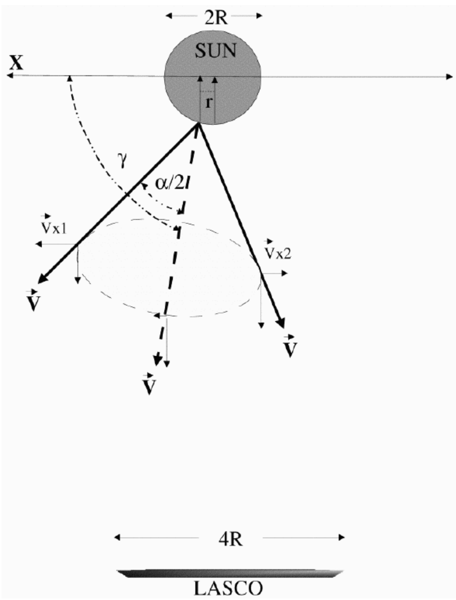


By simple inspection we see from Figure 1 that on the left (eastern) side of the occulting disk, the CME has to trave
a distance $2R$ - $r$ with velocity $V_{x1}$ to appear in coronagraph at time $T_1$ such that

$$T_1 = \frac{(2R-r)}{V_{x1}} .$$

Similarly, the CME will appear on the right (western) side of the occulting disk after a time

$$T_2 = \frac{(2R+r)}{V_{x2}} .$$

From these equations, we determine the time difference

$$\Delta T = T_2 - T_1 = \frac{(2R+r)}{V_{x2}} - \frac{(2R-r)}{V_{x1}} . \quad (1)$$

From the geometry of the CME shown in Figure 1, we get rest of the necessary equations:

$$\cos(\gamma) = \frac{r}{R} , \quad (2)$$

$$\cos\left(\gamma - \frac{\alpha}{2}\right) = \frac{V_{x1}}{V} , \quad (3)$$

$$\cos\left(180^\circ - \gamma - \frac{\alpha}{2}\right) = \frac{V_{x2}}{V} . \quad (4)$$

We have four equations and four parameters to determine $r$, $\alpha$, $V$, and $\gamma$. The inputs $V_{x1}$, $V_{x2}$, and $\Delta T$ need to be obtained from observations. In our considerations, we use data from the *SOHO*/LASCO C2 coronagraph with a

Figure 9.5: Michalek et al. 2003: velocity estimates for halo CMEs that have constant velocities, are symmetric, and propagate with constant angular widths.

- Michalek et al. 2003: A New Method for Estimating Widths, Velocities, and Source Location of Halo Coronal Mass Ejections (ApJ 584, 472)
- Michalek 2006: An Asymmetric Cone Model for Halo Coronal Mass Ejections (Solar Physics, Vol. 237, 101)
- Michalek et al. 2009: Expansion Speed of Coronal Mass Ejections (Solar Physics, Vol. 260, 401)
- Michalek 2010: Is the Asymmetric Cone Model for Halo Coronal Mass Ejections Correct? (Solar Physics, Vol. 261, 107)

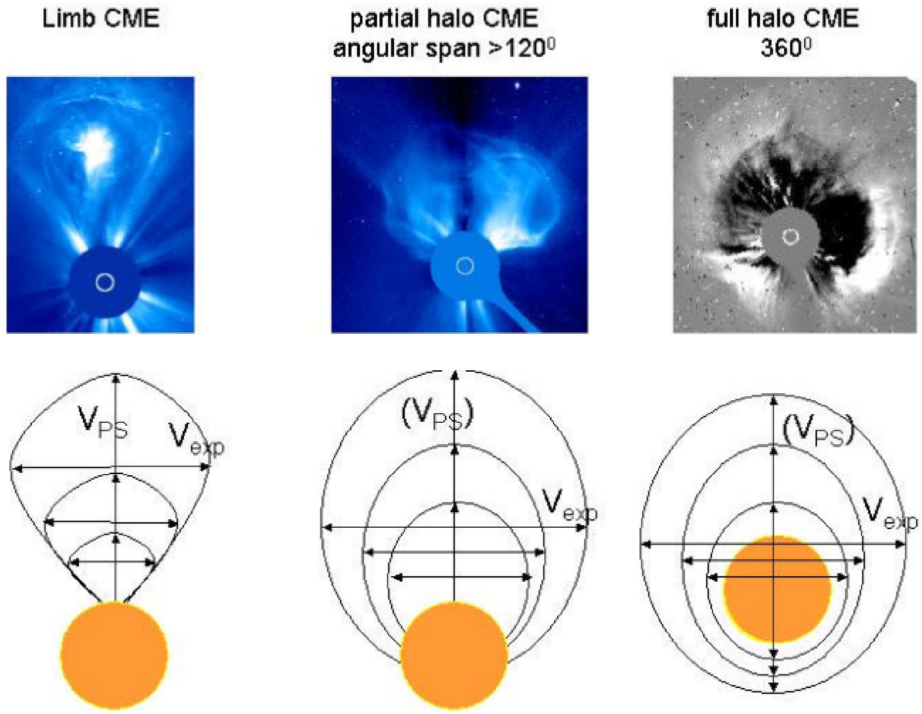


Figure 9.6: Expansion speed ($V_{exp}$) can be determined for all types of CMEs while the apparent plane-of-the-sky speed ($V_{PS}$) contains an unknown speed component towards the observer (Schwenn et al. Ann. Geophys., 23, 1033, 2005).

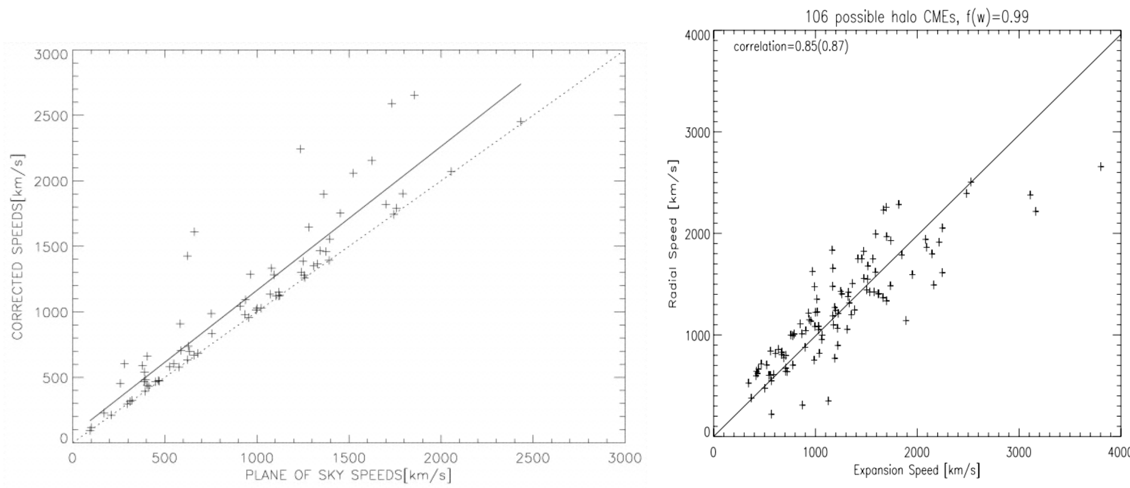


Figure 9.7: Left: plane-of-sky speeds vs. corrected (real) speeds. The solid line shows the linear fit to the data (Michalek et al., 2003). Right: expansion speed (rate of change of the lateral dimension of a CME at its widest part) vs. radial speed (Michalek et al., 2010).

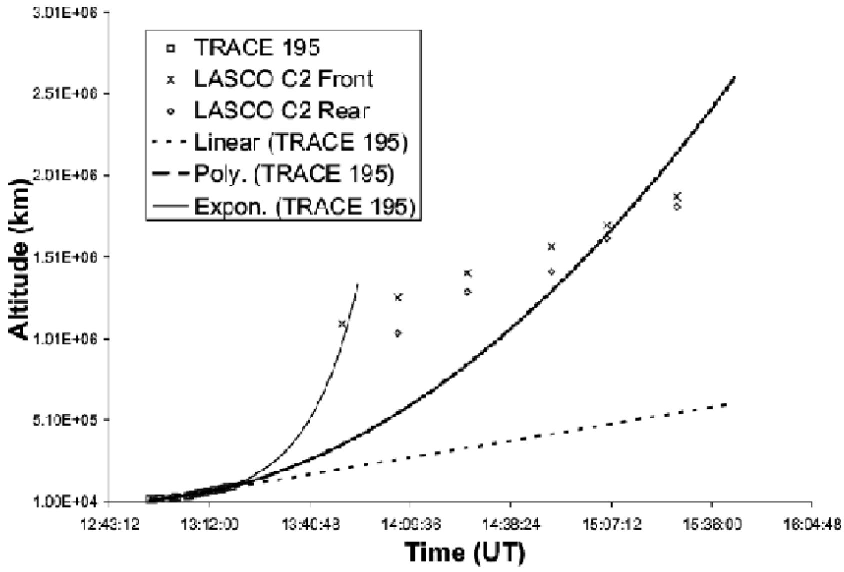


Figure 9.8: CME height-times indicate velocity changes that are difficult to account for (Goff et al., A&A 434, 761, 2005)

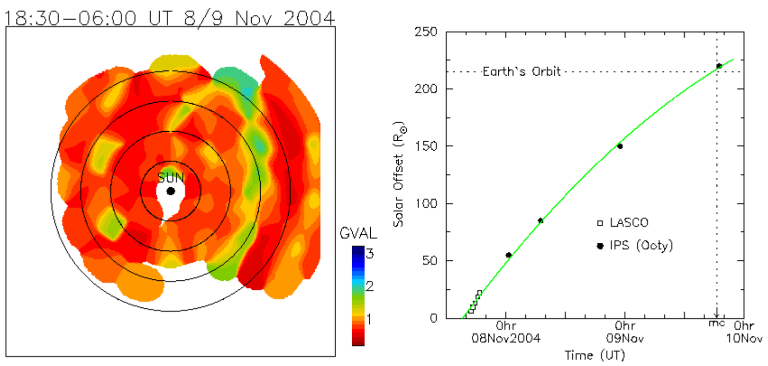


Figure 9.9: At larger distances from the Sun, radio scintillation experiments become useful in estimating CME locations (figures from Manoharan and Pohjolainen et al., 2007).

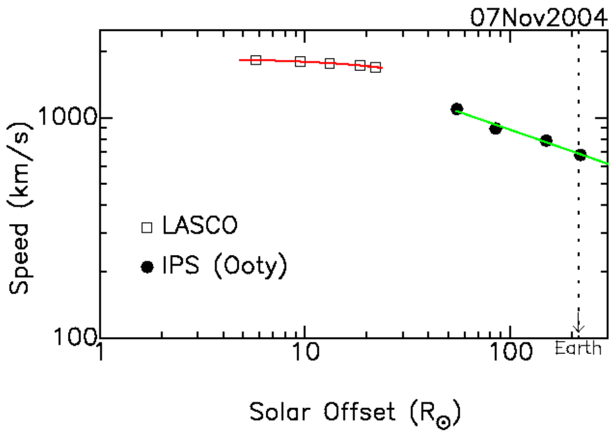


Figure 9.10: Atmospheric drag – or a push when the CME velocity is low and the solar wind speed is high – play a role CME velocity changes

Intensity scintillations of compact radio sources (galaxies or quasars having angular diameter of < 0.5 arcsec) are produced by the density fluctuations in the solar wind plasma. The presence of solar wind transients (e.g., CMEs) can be identified by the enhanced g-values (normalized scintillation index) which are due to the increase in the density-fluctuation (i.e., turbulence) level. Radio observations are made in Ooty (India) and Nagoya (Japan) at 327 MHz (Manoharan et al. 2001).

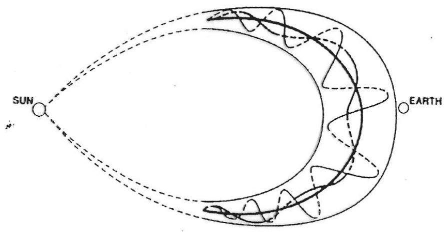


Figure 9.11: The footpoints of magnetic clouds can stay attached to the Sun quite a long time after eruption (Kallenrode, Space Physics).

Questions related to flares and CMEs:

- How does the energy needed for eruption build up? (observations of 'inflow'?)
- How does the magnetic field open up? (from the inside or the outside?)
- What can affect the particles/magnetic clouds during their travel? (solar wind anisotropies, CME interaction, etc.)

There are still open issues:

- There are CMEs with and without flares
- Filament eruptions do not always produce CMEs
- CME speeds are surprisingly different: 10...3000 km/s
- CMEs can accelerate/decelerate suddenly
- Energetic particles (observed in situ near Earth) are produced somewhere along the processes (flare-accelerated vs. CME-accelerated)

and questions to be answered:

- How do filaments and flares fit in the picture of CME formation?
  What is the cause and what are the effects?
- Can we really say when a CME "starts"?
- The old classification, filament eruption -> slow CME, and flare -> fast CME, can be questioned?
- When and how do CMEs accelerate/decelerate?
  In the SOHO era there has been an observational gap between 1.3-2.1 $R_{sun}$, but STEREO observations could now give some more information.

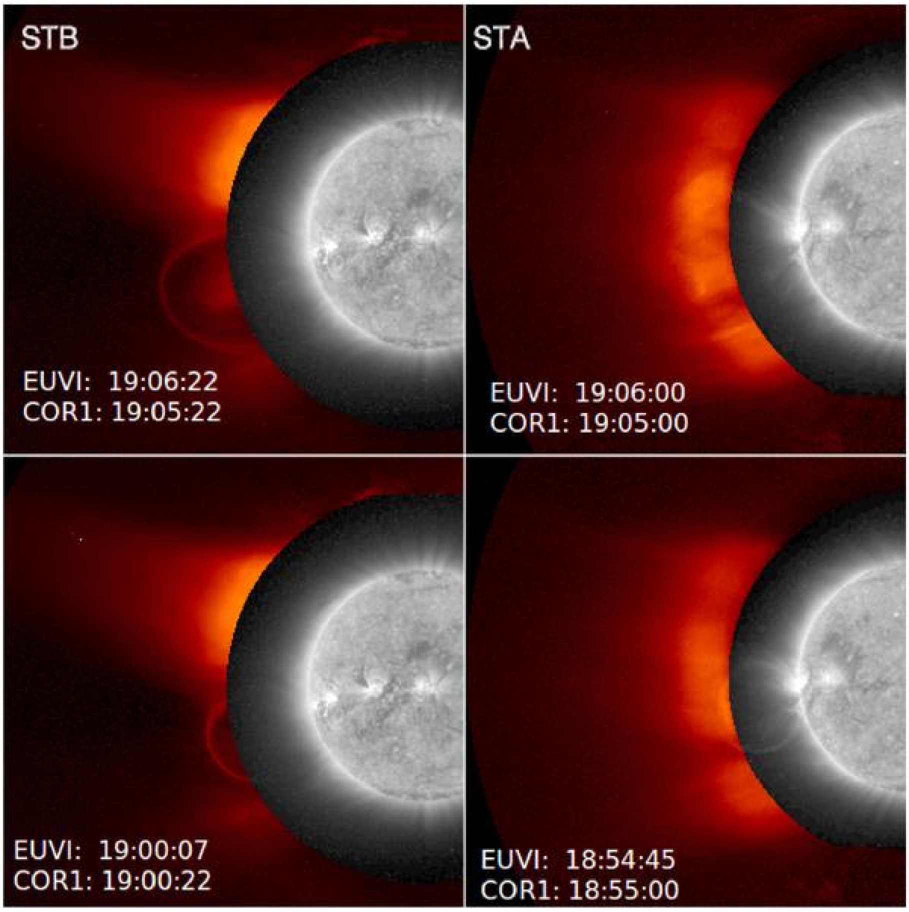


Figure 9.12: STEREO A and B observations of the emergence of an EUVI bubble into the COR1 field of view, where it becomes the cavity of a typical three-part CME (Patsourakos et al. A&A 522, 2010).

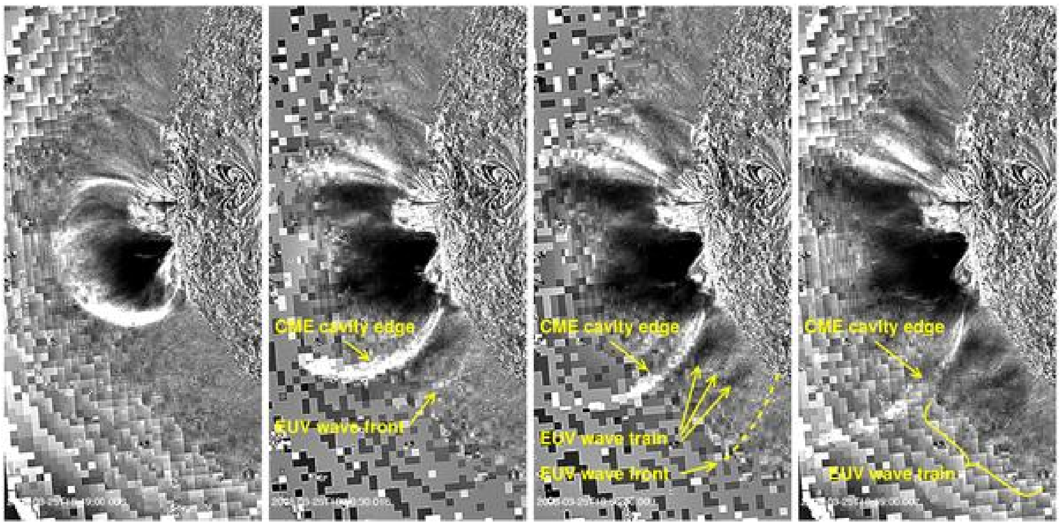


Figure 9.13: Launch of an EUV wave by the horizontal (over)expansion of the CME cavity (Patsourakos et al. A&A 522, 2010).

## 9.2 Dimmings

Dimming regions are identified by their strong depletion in coronal EUV emission within ~ half hour of the estimated time of CME lift-off. They include areas which are as dark as quiescent coronal hole areas, as well as other regions with weaker brightness depletions. The extended dimming areas in analysed events generally map out the apparent “foot-print” of a CME, as observed by white-light coronagraphs (see more details in Thompson et al., Geophysical Research Letters, 2000).

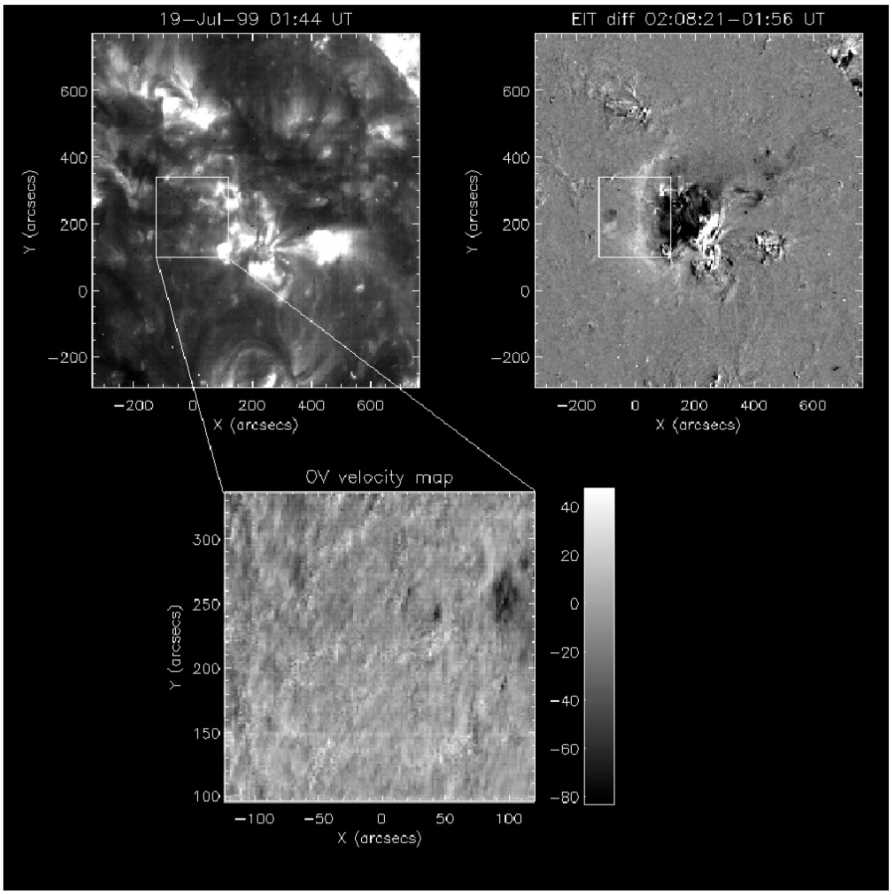


Figure 9.14: Evidence of CME launch: rising material is observed in blueshift in chromospheric spectral lines (Harra & Sterling, 2001)

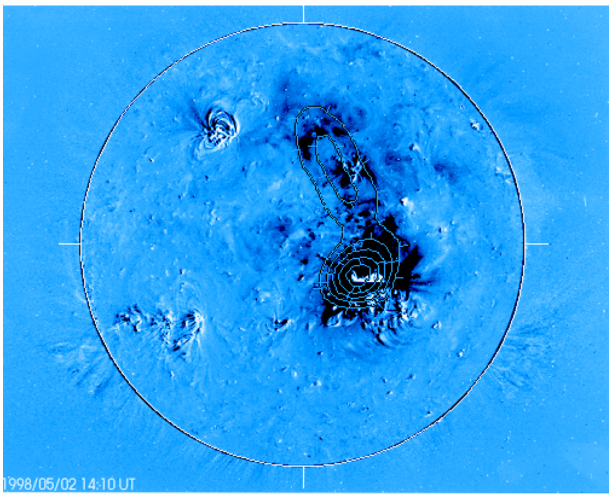


Figure 9.15: Radio sources have been found to match with disappearing features: in this case radio type IV emission (interpreted as emission from trapped particles within a magnetic cloud) was observed over an EUV dimmed region (Pohjolainen et al., 2001)

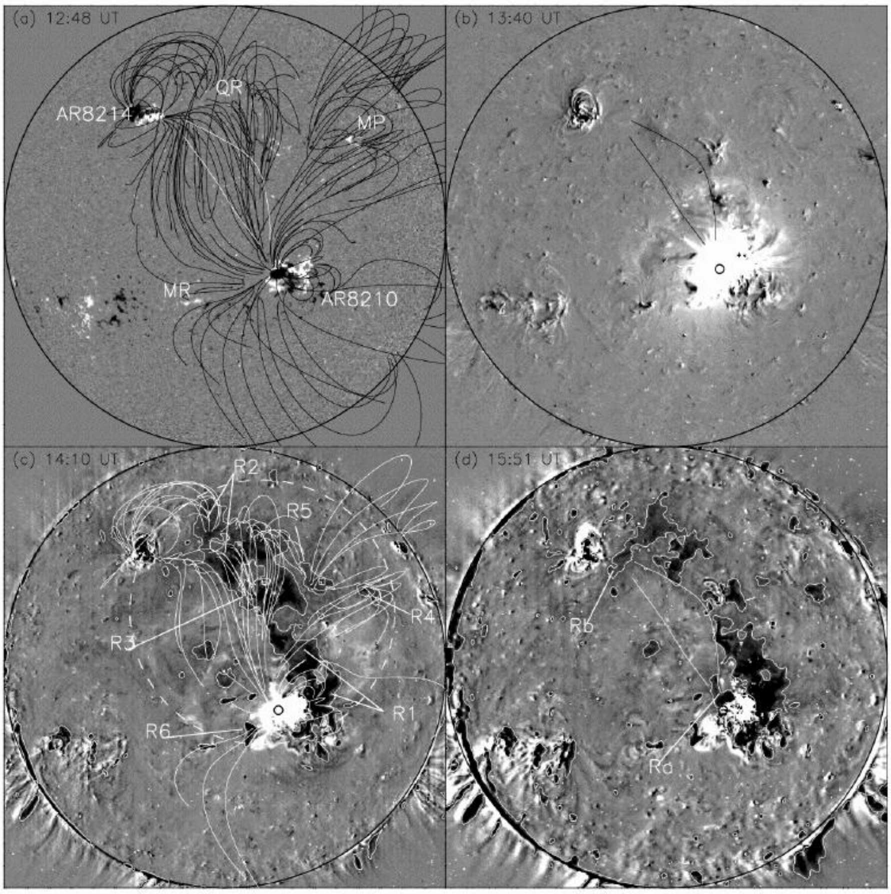


Figure 9.16: Magnetic field extrapolations verify the locations and connections of loops which are later found to disappear (Wang et al., 2002). Remember that structures are visible only if their temperatures and densities fall within those of the observing instruments.

The sudden dimming of parts of the corona, as observed in soft X-rays, can be recognized as (see Yohkoh Science Nugget December 10, 1999, by Hugh Hudson):
- Transient coronal holes (discovered with Skylab observations)
- Above-the-arcade dimming
- Enveloping dimming
- Moving cloud
- Disappearing trans-equatorial (large-scale) loops

Disappearance may also mean that the structure expands (electron density decreases) and cools down, and therefore it is no longer detected by the instrument. We can estimate the time scales with

$$\tau_{rad} = \frac{3kT}{\Lambda n_e} \sim 10^5 \text{ s} \sim \texttt{1day}, \tag{9.1}$$

$\Lambda$=3x$10^{-23}$ erg cm$^3$ s$^{-1}$,

$$\tau_{cond} = \frac{2nkl^2}{\kappa_0 T^{2.5}} \sim 10^4 \text{ s} \sim \texttt{3hours}, \tag{9.2}$$

$\kappa_0 = 10^{-6}$ erg (cm K$^{3.5}$)$^{-1}$.

Mass estimate for the moving and disappearing soft X-ray cloud was $4 \times 10^{14}$ g, which corresponds to a small coronal mass ejection. The observed movement was $\sim$ 100 km/s (too slow to create any shock waves). The observed timescale for the disappearing SXT structure was $< 3 \times 10^3$ s (uncertainty due to Yohkoh entering satellite night time at the wrong moment!), so the disappearance could not be due to heat transfer by radiation or conduction.

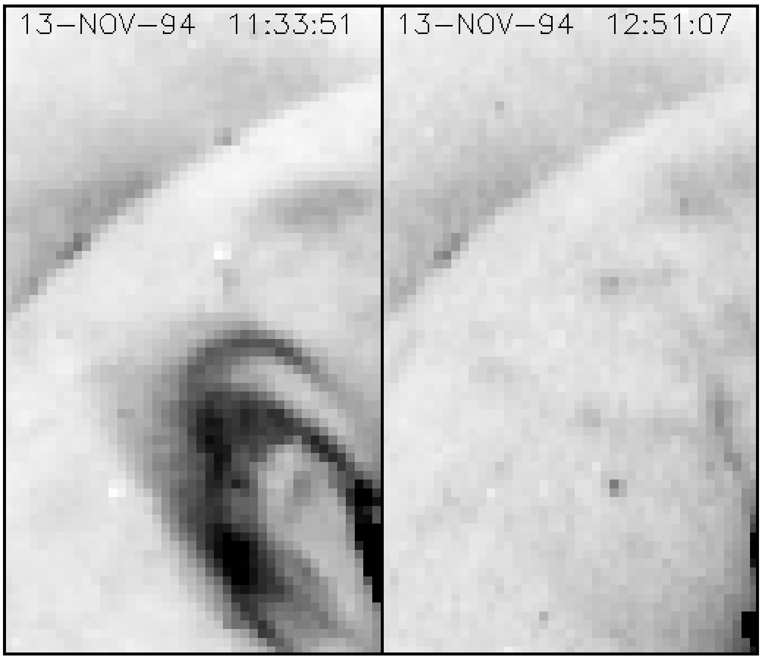


Figure 9.17: Disappearing SXT cloud (H. Hudson, Yohkoh Science Nuggets)

## 9.3 CMEs, filaments, type IIs, and flares - all connected?

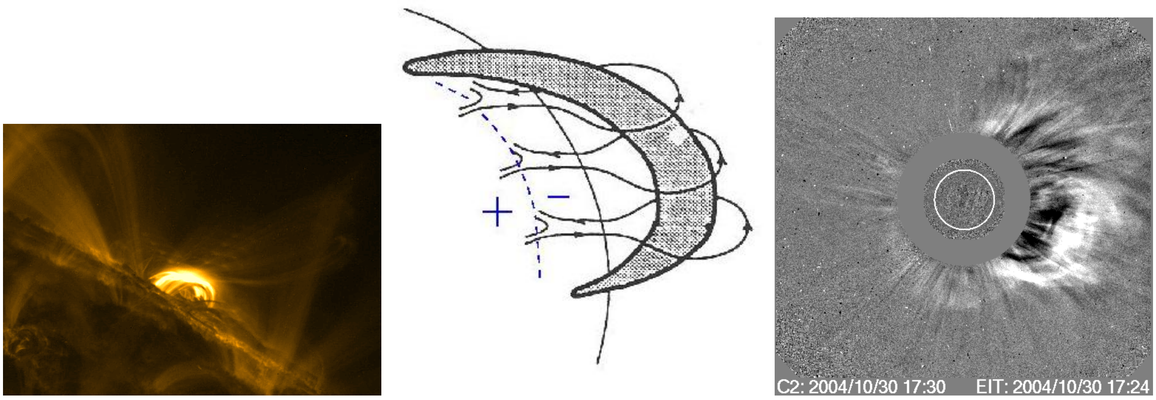


Figure 9.18: Are flares, filament eruptions and CMEs always connected?

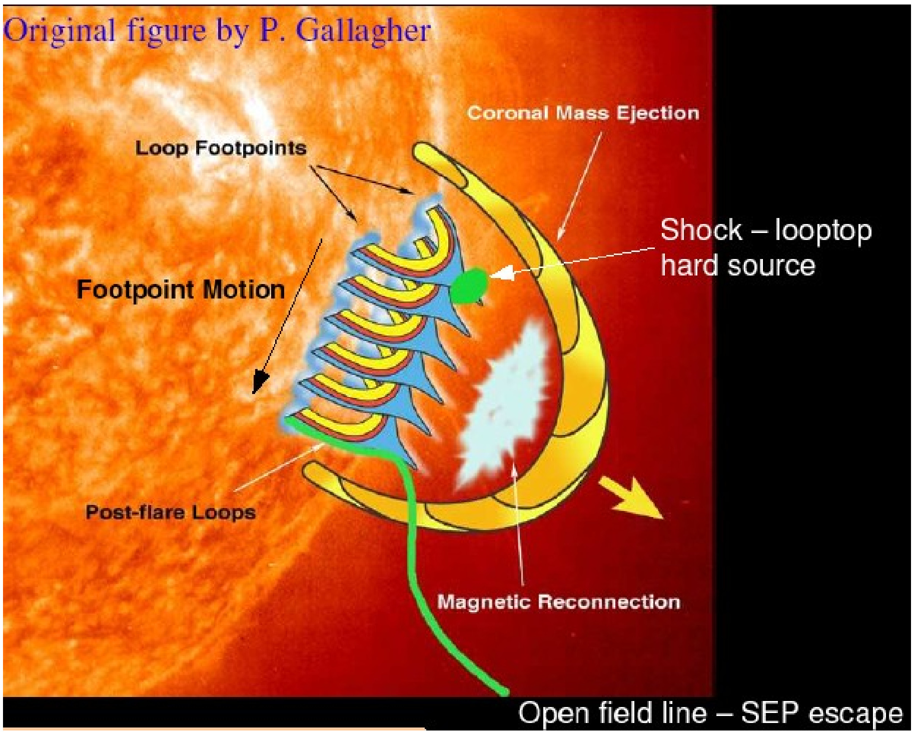


Figure 9.19: Unifield models can explain all features! (Smith & Gallagher, 2004).

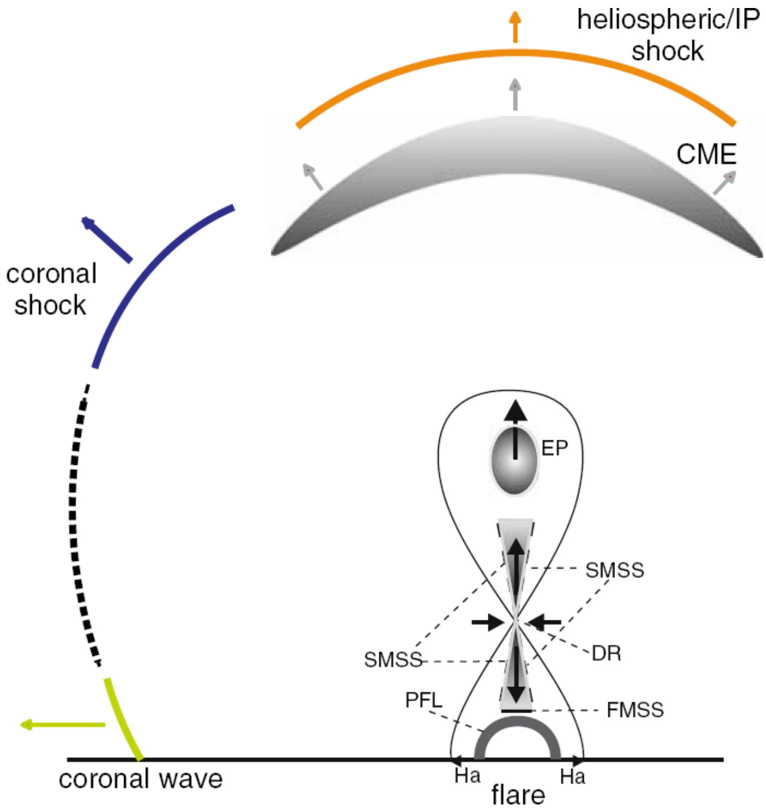


Figure 9.20: ... even shocks? (Warmuth, LNP 2007/ Aurass et al., A&A 2002)

Things to evaluate in type II burst emission:

- Atmospheric density models -> speed from density change
- Scale height + frequency drift -> may give different speed
- Corona: second harmonic stronger
- IP space: fundamental stronger
- Emission lanes can be band-split
- May not be plasma emission at all

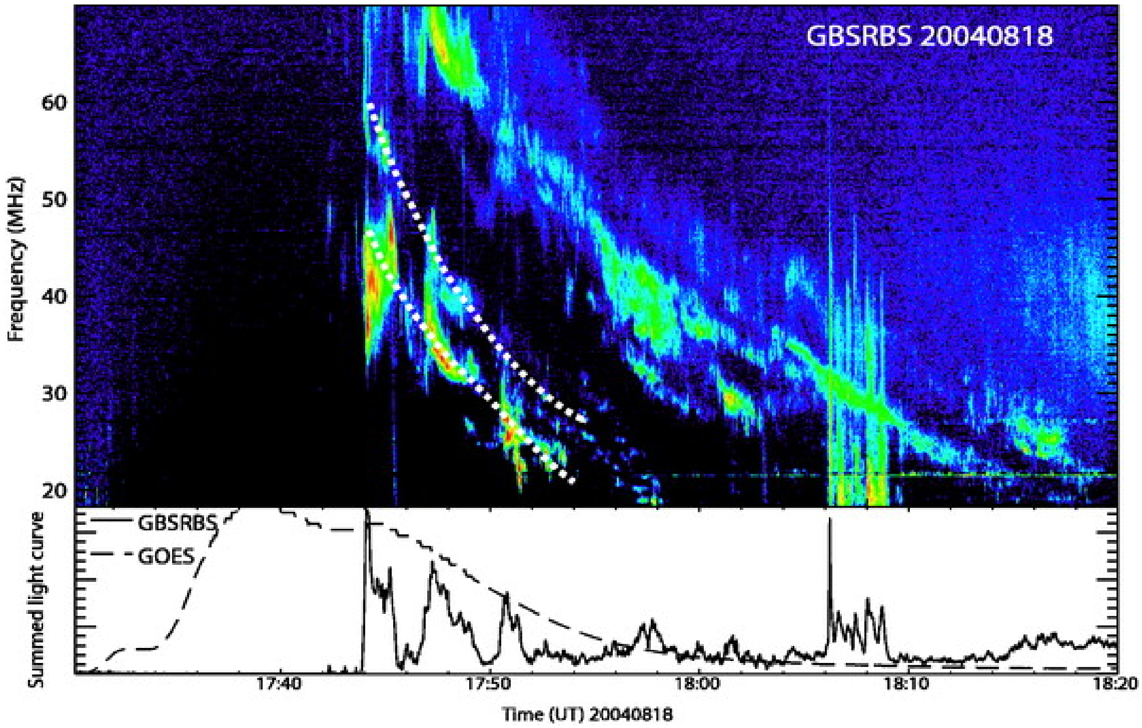


Figure 9.21: Emission at the upper (HFB) and lower (LFB) frequency branches in the fundamental band of the type II burst (dotted lines). Band-split reveals the shock Mach number if it is a consequence of the plasma emission from the upstream and downstream shock region. Shock speed can be inferred from the frequency drift $\rightarrow$ Alfvén velocity and magnetic field can be estimated (Cho et al. ApJ 665, 799, 2007; Vrsnak et al. ESA SP-506, 2002).

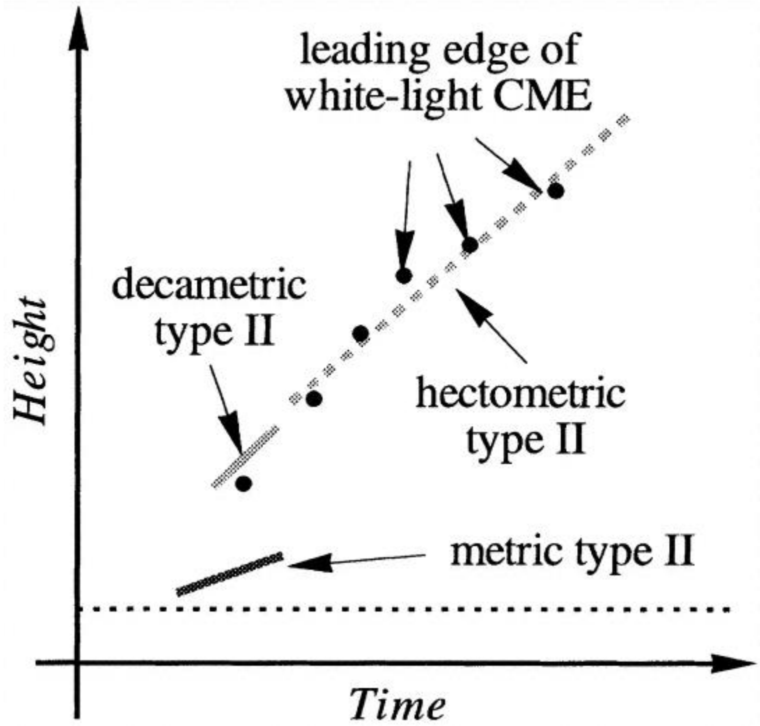


Figure 9.22: A unified model? (Magara et al. ApJ, 538, L175, 2000)

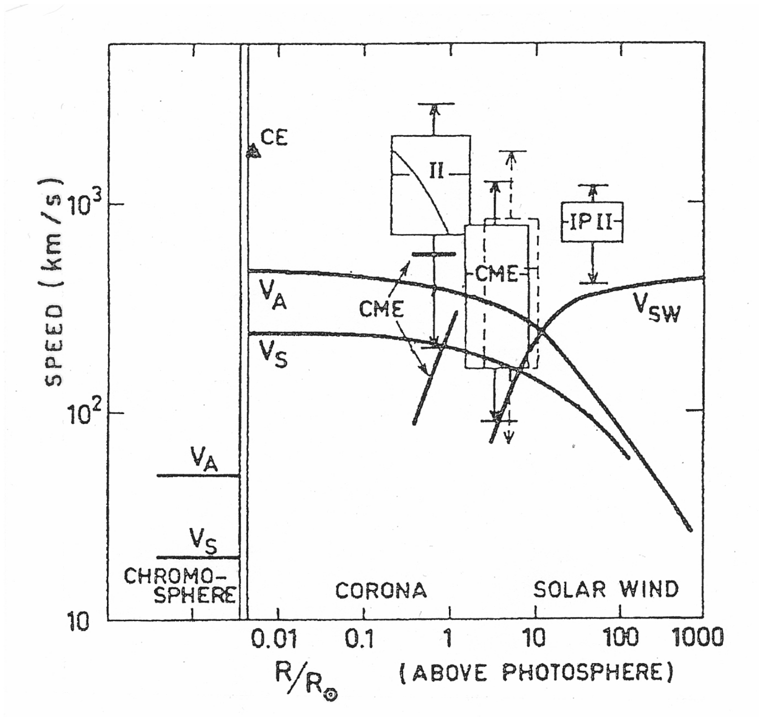


Figure 9.23: Observations of coronal type II, interplanetary (IP) type II, and CME speeds, compared to the Alfven speed, sound speed, and solar wind speed (Kallenrode: Space Physics).

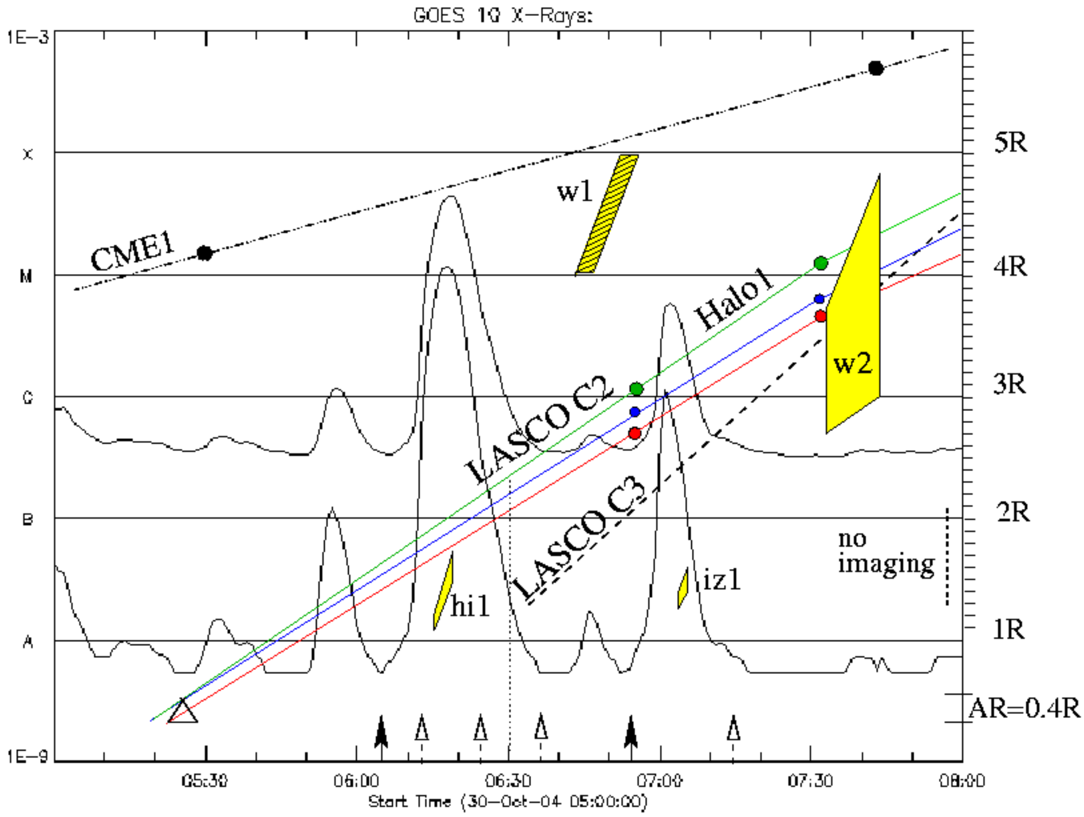


Figure 9.24: There are many studies that try to combine and interpret all available observations. This example from Pohjolainen & Lehtinen (2006) shows data for one halo CME event. The estimated heliocentric CME heights, in solar radii (R) along the selected radials, are plotted over the GOES X-ray flux curve. An extrapolated linear fit on the height-times from the later LASCO C3 observations is also shown. Vertical dotted line shows the time of the earlier LASCO C2 observation when the CME could have been observed if it was within the field of view. The height-times of the preceding CME1 are also shown. Type II burst times and estimated heights (height ranges defined by using 2-fold Newkirk and 2-fold Saito coronal density models) are marked in the plot: "hi1" denotes Hiras observations where fundamental emission starts at 06:15 UT at 150 MHz, "iz1" denotes Izmiran observations where fundamental emission starts at 06:42 UT at 90 MHz, "w1" denotes WIND RAD2 observations of a DH type II burst starting at 06:42 UT at 3.2 MHz, and "w2" denotes a burst starting at 07:32 UT at 10 MHz. Triangle indicates the time of an H$\alpha$ filament eruption around 05:25 UT. The Yunnan observations were limited due to bad weather conditions, but there is some indication of another filament eruption near 06:26 UT. Black arrow shows the start times of two GOES flares at 06:04 and 06:54 UT, and dashed arrows show the times when EIT dimmings were observed (note that there were no available 195 Å EIT images near the start of the second flare, between 06:48 and 07:13 UT). The EIT field of view ends at height ≈ 1.3 R and the LASCO C2 field of view begins around 2.1 R, and thus there is a wide range of heights where imaging is not available. The flaring active region and the dimmed areas were located approximately at 0.4-0.6 R on the disk. This study found support that the cause of metric type II bursts, for two of the analysed three events, was flare-related.

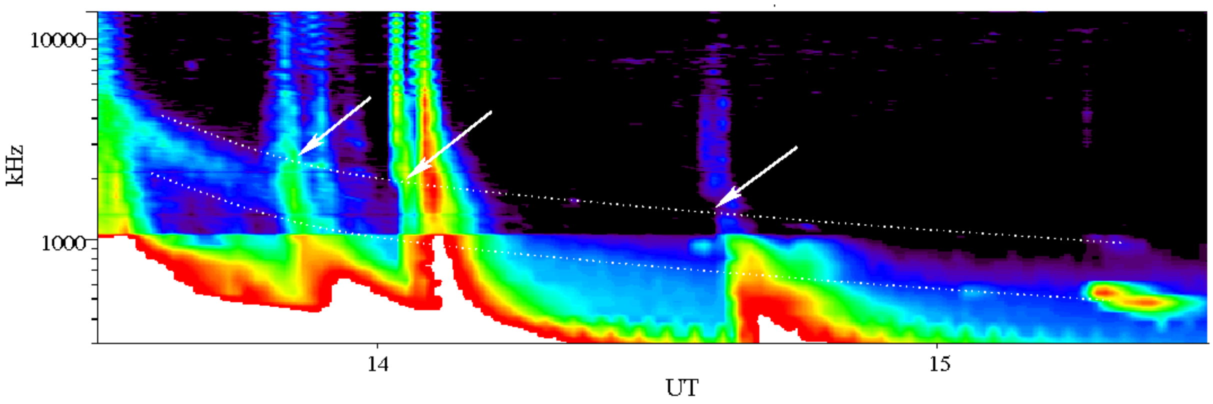


Figure 9.25: Shocks on the way: tilted type III burst lanes (Lehtinen et al., 2008).

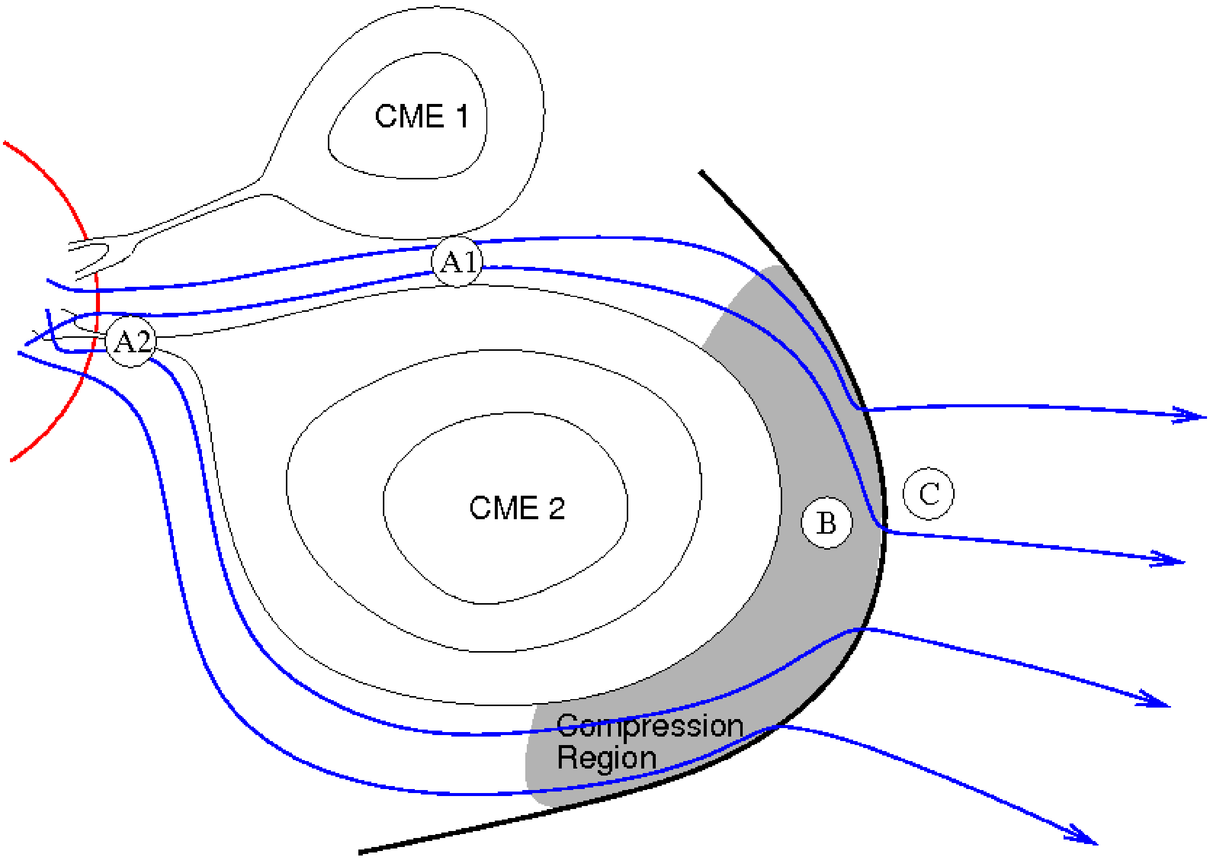


Figure 9.26: Tilts could be due to electron streams passing through shock fronts.

Complex Type III Radio Emissions 343

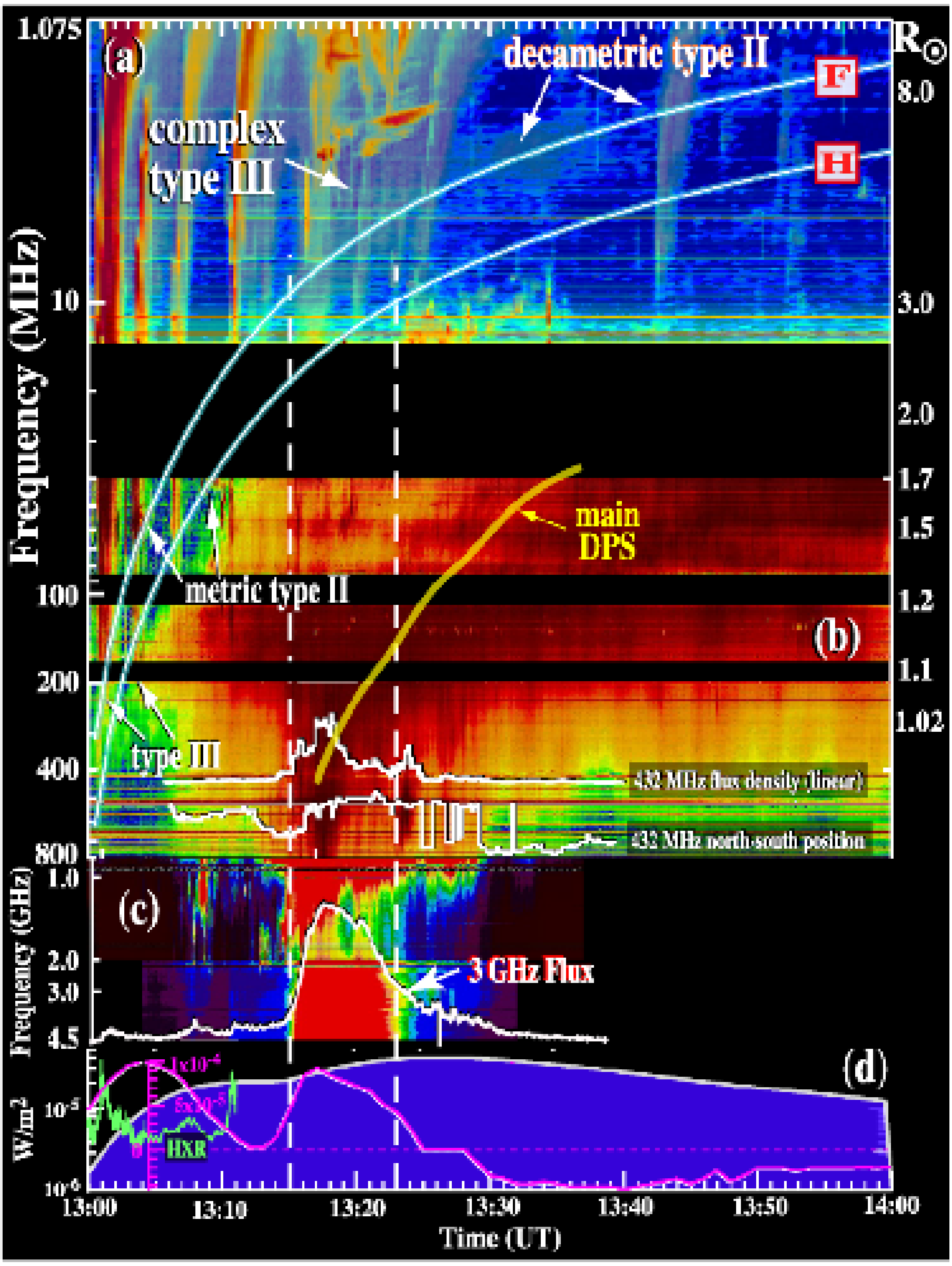


Figure 9.27: Reiner et al., 2008 (see also Hilary Cane and shock-accelerated 'SA-events')

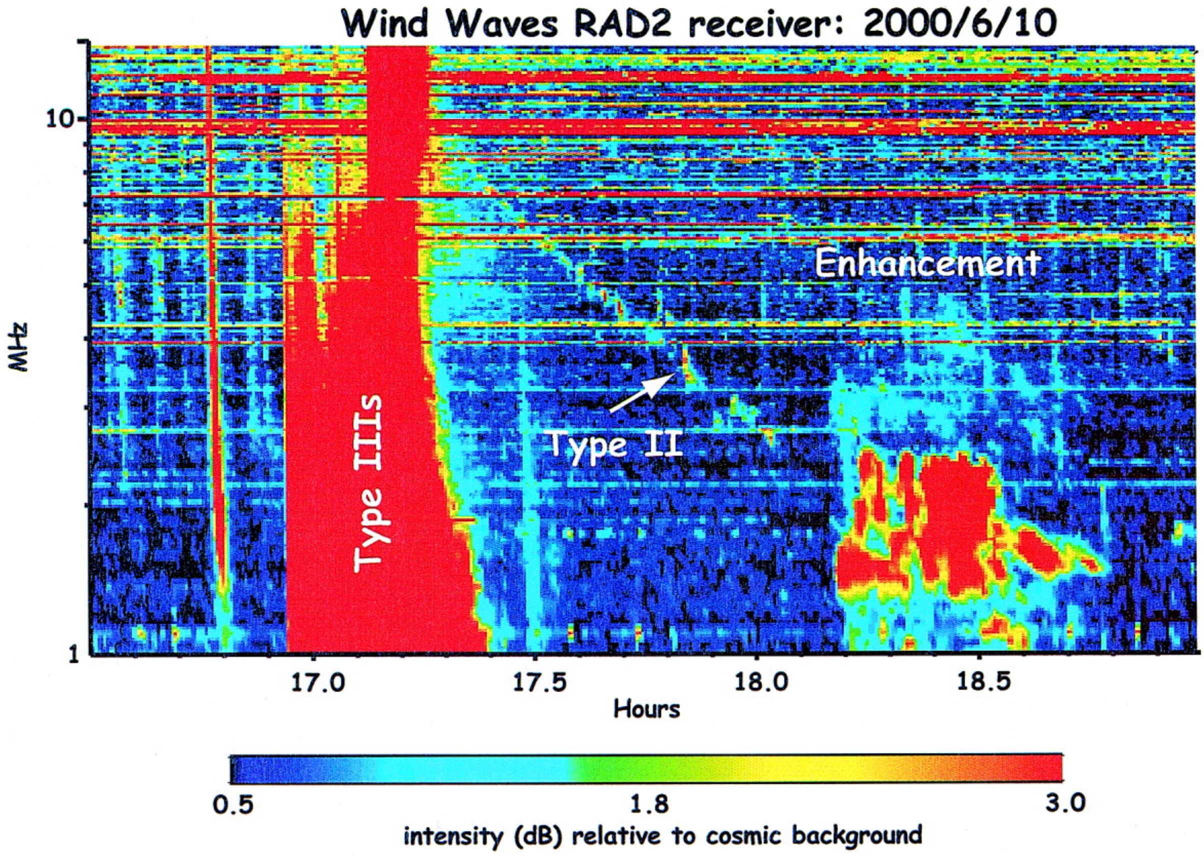


Figure 9.28: Radio features from interacting CMEs? (Gopalswamy et al. ApJ, 2001)

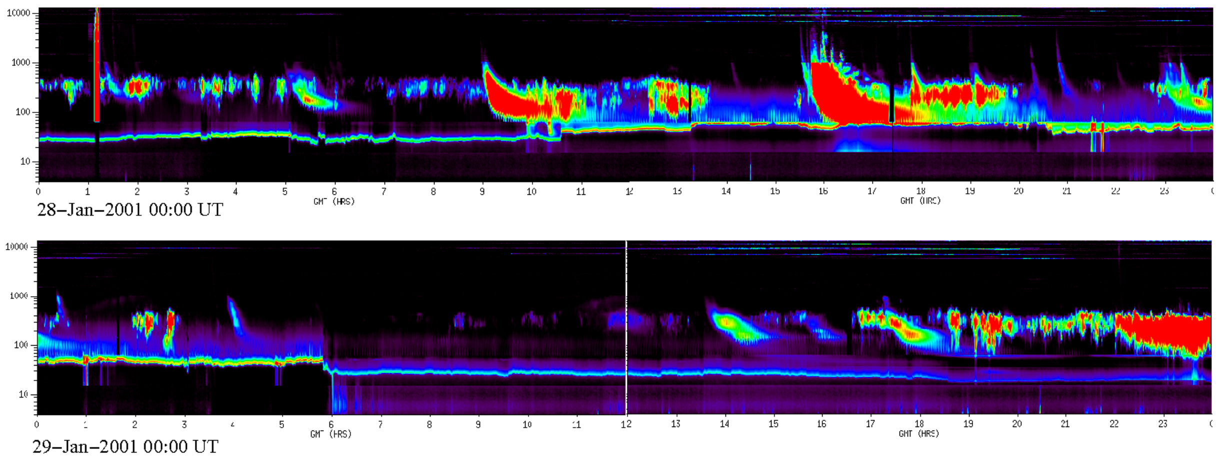


Figure 9.29: AKR - auroral kilometric radiation - appears usually at 80 – 400 kHz causing radiation episodes every 12 hours that affect observations of radio emission originating from the Sun.

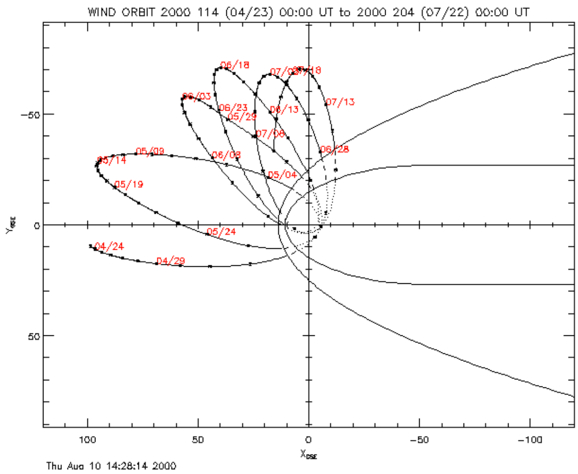


Figure 9.30: Wind WAVES orbit takes the satellite near Earth – and AKR gets more intense.

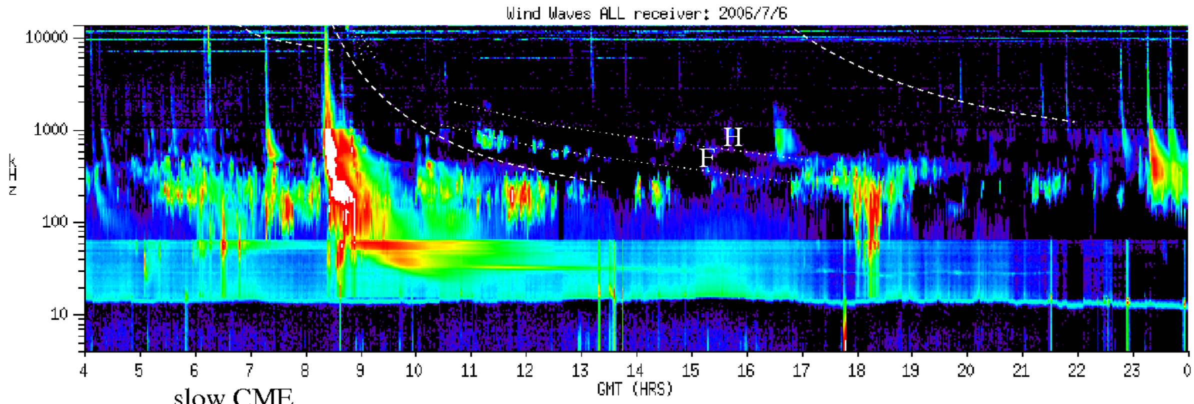


Figure 9.31: Radio emission in the IP space can consist of propagating CMEs, type II shocks, type III bursts, and AKR, all mixed together.

**Statistics on CMEs, type IIs, and flares:**

- 2/3 of metric type IIs are accompanied by fast CMEs
- 2/5 of CMEs are without metric type IIs
- 1/2 of CMEs without metric type IIs are fast CMEs (> 450 km/s)
- 90% of flares are without CMEs
- 60% of CMEs are without flares
- Energy realeased in a CME is larger than in a flare
- In 65% of CME–flare events the CME starts first